A New Modeling of the Macpherson Suspension System and its Optimal Pole-Placement Control

Keum-Shik Hong*
School of Mechanical Engineering
Pusan National University
Pusan, 609-735 Korea

Dong-Seop Jeon**
Graduate College
Pusan National University
Pusan, 609-735 Korea

Hyun-Chul Sohn‡
Graduate College
Pusan National University
Pusan, 609-735 Korea

Abstract

In this paper a new model and an optimal pole-placement control for the Macpherson suspension system are investigated. The focus in this new modeling is the rotational motion of the unsprung mass. The two generalized coordinates selected in this new model are the vertical displacement of the sprung mass and the angular displacement of the control arm. The vertical acceleration of the sprung mass is measured, while the angular displacement of the control arm is estimated. It is shown that the conventional model is a special case of this new model since the transfer function of this new model coincides with that of the conventional one if the lower support point of the damper is located at the mass center of the unsprung mass. It is also shown that the resonance frequencies of this new model agree better with the experimental results. Therefore, this new model is more general in the sense that it provides an extra degree of freedom in determining a plant model for control system design. An optimal pole-placement control which combines the LQ control and the pole-placement technique is investigated using this new model. The control law derived for an active suspension system is applied to the system with a semi-active damper, and the performance degradation with a semi-active actuator is evaluated. Simulations are provided.

1 Introduction

In this paper, a new model of the suspension system of the Macpherson type for control system design and an optimal pole-placement control for the new model are investigated. The roles of a suspension

* Email: *kshong@hyowon.pusan.ac.kr.*
** E-mail: *dosjeon@hyowon.pusan.ac.kr.*
‡ E-mail: *hcson@hyowon.pusan.ac.kr.*

system are to support the weight of the vehicle, to isolate the vibrations from the road, and to maintain the traction between the tire and the road. The suspension systems are classified into passive and active systems according to the existence of a control input. The active suspension system is again subdivided into two types: a full active and a semi-active system based upon the generation method of the control force. The semi-active suspension system produces the control force by changing the size of an orifice, and therefore the control force is a damping force. The full active suspension system provides the control force with a separate hydraulic power source. In addition, the suspension systems can be divided, by their control methods, into a variety of types: In particular, an adaptive suspension system is the type of suspension system in which controller parameters are continuously adjusted by adapting the time-varying characteristics of the system. Adaptive methods include a gain scheduling scheme, a model reference adaptive control, a self-tuning control, etc.

The performance of a suspension system is characterized by the ride quality, the drive stability, the size of the rattle space, and the dynamic tire force. The prime purpose of adopting an active suspension system is to improve the ride quality and the drive stability. To improve the ride quality, it is important to isolate the vehicle body from road disturbances, and to decrease the resonance peak at or near 1 Hz which is known to be a sensitive frequency to the human body.

Since the sky-hook control strategy, in which the damper is assumed to be directly connected to a stationary ceiling, was introduced in the 1970's, a number of innovative control methodologies have been proposed to realize this strategy. Alleyne and Hedrick[3] investigated a nonlinear control technique which combines the adaptive control and the variable structure control with an experimental electro-hydraulic suspension system. In their research, the performance of the controlled system was evaluated by the ability of the actuator output to track the specified skyhook force. Kim and Yoon[4] investigated a semi-active control law that reproduces the control force of an optimally controlled active suspension system while de-emphasizing the damping coefficient variation. Truscott and Wellstead[5] proposed a self-tuning regulator that adapts the changed vehicle conditions at start-up and road disturbances for active suspension systems based on the generalized minimum variance control. Teja and Srinivasa[6] investigated a stochastically optimized PID controller for a linear quarter car model.

Compared with various control algorithms in the literature, research on models of the Macpherson strut wheel suspension are rare. Stensson et al.[8] proposed three nonlinear models for the Macpherson strut wheel suspension for the analysis of motion, force and deformation. Jonsson[7] conducted a finite element analysis for evaluating the deformations of the suspension components. These models would be appropriate for the analysis of mechanics, but are not adequate for control system design. In this paper, a new control-oriented model is investigated.

Fig. 1 shows a sketch of the Macpherson strut wheel suspension. Fig. 2 depicts the conventional quarter car model of the Macpherson strut wheel suspension for control system design. In the

conventional model, only the up-down movements of the sprung and the unsprung masses are incorporated. As are shown in Fig. 1 and Fig. 3, however, the sprung mass, which includes the axle and the wheel, is also linked to the car body by a control arm. Therefore, the unsprung mass can rotate besides moving up and down. Considering that better control performance is being demanded by the automotive industry, investigation of a new model that includes the rotational motion of the unsprung mass and allows for the variance of suspension types is justified.

The Macpherson type suspension system has many merits, such as an independent usage as a shock absorber and the capability of maintaining the wheel in the camber direction. The control arm plays several important roles: it supports the suspension system as an additional link to the body, completes the suspension structure, and allows the rotational motion of the unsprung mass. However, the function of the control arm is completely ignored in the conventional model.

In this paper, a new model which includes a sprung mass, an unsprung mass, a coil spring, a damper, and a control arm is introduced for the first time. The mass of the control arm is neglected. For this model, the equations of motion are derived by the Lagrangian mechanics. The open loop characteristics of the new model is compared to that of the conventional one. The frequency responses and the natural frequencies of the two models are analyzed under the same conditions. Then, it is shown that the conventional 1/4 car model is a special case of the new model. An optimal pole-placement control, which combines the LQ control and the pole-placement technique, is applied to the new model. The closed loop performance is analyzed. Finally, the optimal pole-placement law, derived for the active suspension system, is applied to the semi-active suspension system which is equipped with a continuously variable damper for the purpose of investigating the degradation of the control performance.

The results in this paper are summarized as follows. A new model for the Macpherson type suspension system that incorporates the rotational motion of the unsprung mass is suggested for the first time. If the lower support point of the shock absorber is located at the mass center of the unsprung mass, the transfer function, from road disturbance to the acceleration of the sprung mass, of the new model coincides with that of the conventional one. Therefore, the new model is more general, from the point of view that it can provide an extra degree of freedom in determining a plant model for control design purpose. In the frequency response analysis, the natural frequencies of the new model agree better with the experimental results. An optimal pole-placement control, which combines the LQ control and the pole-placement technique, is applied to the new model. The control law, derived for a full active suspension, is applied to the semi-active system with a continuously variable damper. It is shown that a small degradation of control performance occurs with a continuously variable damper.

2. Conventional Model

Fig. 2 shows the conventional model that depicts the vertical motions of the sprung and the unsprung masses. All coefficients in Fig. 2 are assumed to be linear. The equations of motion are

$$\begin{aligned} m_s\ddot{z}_s &= -k_s(z_s - z_u) - c_p(\dot{z}_s - \dot{z}_u) + f_a - f_d \\ m_u\ddot{z}_u &= k_s(z_s - z_u) + c_p(\dot{z}_s - \dot{z}_u) + k_t(z_u - z_r) - f_a \end{aligned} \tag{1}$$

The state variables are defined as: $x_1 = z_s - z_u$, the suspension deflection; $x_2 = \dot{z}_s$, the velocity of the sprung mass; $x_3 = z_u - z_r$, the tire deflection; $x_4 = \dot{z}_u$, the velocity of the unsprung mass[10]. Then, the state equation is

$$\dot{x} = Ax + B_1 f_a + B_2 \dot{z}_r + B_3 f_d \tag{2}$$

where,

$$A = \begin{bmatrix} 0 & 1 & 0 & -1 \\ -\frac{k_s}{m_s} & -\frac{c_p}{m_s} & 0 & \frac{c_p}{m_s} \\ 0 & 0 & 0 & 1 \\ \frac{k_s}{m_s} & \frac{c_p}{m_u} & -\frac{k_t}{m_u} & -\frac{c_p}{m_u} \end{bmatrix}, \quad B_1 = \begin{bmatrix} 0 & \frac{1}{m_s} & 0 & -\frac{1}{m_u} \end{bmatrix}^T, B_2 = \begin{bmatrix} 0 & 0 & -1 & 0 \end{bmatrix}^T, B_3 = \begin{bmatrix} 0 & \frac{1}{m_s} & 0 & 0 \end{bmatrix}^T.$$

And, the transfer function from the road input $\dot{z}_r$ to the acceleration of the sprung mass is.

$$H_a(s) = \frac{\ddot{z}_s(s)}{\dot{z}_r(s)} = \frac{k_t s(c_p s + k_s)}{d(s)} \tag{3}$$

where

$$\begin{aligned} d(s) = {} & m_s m_u s^4 + (m_s + m_u)c_p s^3 + \{(m_s + m_u)k_s + m_s k_t\}s^2 \\ & + k_t c_p s + k_s k_t \end{aligned}.$$

3. A New Model

The schematic diagram of the Macpherson type suspension system is shown in Fig. 3. It is composed of a quarter car body, an axle and a tire, a coil spring, a damper, an axle, a load disturbance and a control arm. The car body is assumed to have only a vertical motion. If the joint between the control arm and the car body is assumed to be a bushing and the mass of the control arm is not neglected, the degrees of freedom of the whole system is four. The generalized coordinates in this case are z_s, d, q_1 and q_2. However, if the mass of the control arm is ignored and the bushing is assumed to be a pin joint, then the degrees of freedom becomes two.

As the mass of the control arm is much smaller than those of the sprung mass and the unsprung mass, it can be neglected. Under the above assumption, a new model of the Macpherson type suspension system is introduced in Fig. 4. The vertical displacement z_s of the sprung mass and the

rotation angle q of the control arm are chosen as the generalized coordinates. The assumptions adopted in Fig. 4 are summarized as follows.

1. The horizontal movement of the sprung mass is neglected, i.e. the sprung mass has only the vertical displacement z_s.

2. The unsprung mass is linked to the car body in two ways. One is via the damper and the other is via the control arm. q denotes the angular displacement of the control arm.

3. The values of z_s and q will be measured from their static equilibrium points.

4. The sprung and the unsprung masses are assumed to be particles.

5. The mass and the stiffness of the control arm are ignored.

6. The coil spring deflection, the tire deflection and the damping forces are in the linear regions of their operating ranges.

Let (y_A, z_A), (y_B, z_B) and (y_C, z_C) denote the coordinates of point A, B and C, respectively, when the suspension system is at an equilibrium point. Let the sprung mass be translated by z_s upward, and the unsprung mass be rotated by q in the counter-clockwise direction. Then, the following equations hold.

$$y_A = 0 \tag{4a}$$

$$z_A = z_s \tag{4b}$$

$$y_B = l_B(\cos(q - q_0) - \cos(-q_0)) \tag{4c}$$

$$z_B = z_s + l_B(\sin(q - q_0) - \sin(-q_0)) \tag{4d}$$

$$y_C = l_C(\cos(q - q_0) - \cos(-q_0)) \tag{4e}$$

$$z_C = z_s + l_C(\sin(q - q_0) - \sin(-q_0)) \tag{4f}$$

where q_0 is the initial angular displacement of the control arm at an equilibrium point. Let $a' = a + q_0$. Then, the following relations are obtained from the triangle OAB.

$$l = (l_A^2 + l_B^2 - 2l_A l_B \cos a')^{\frac{1}{2}}$$

$$l' = (l_A^2 + l_B^2 - 2l_A l_B \cos(a' - q))^{\frac{1}{2}}$$

where l is the initial distance from A to B at an equilibrium state, and l' is the changed distance from A to B with the rotation of the control arm by q. Therefore, the deflection of the spring, the relative velocity of the damper and the deflection of the tire are, respectively

$$\begin{aligned}(\Delta l)^2 &= (l - l')^2 \\ &= 2a_l - b_l(\cos a' + \cos(a' - q)) - 2\{a_l^2 - a_l b_l \cdot \\ &\quad (\cos a' + \cos(a' - q) + b_l^2 \cos a' \cos(a' - q)\}^{\frac{1}{2}}\end{aligned} \tag{5a}$$

$$\dot{\Delta l} = \dot{l} - \dot{l}' = \frac{b_l \sin(a' - q)\dot{q}}{2(a_l - b_l \cos(a' - q))^{1/2}} \tag{5b}$$

$$z_C - z_r = z_s + l_C(\sin(q - q_0) - \sin(-q_0)) - z_r \tag{5c}$$

where, $a_l = l_A^2 + l_B^2$, $b_l = 2l_A l_B$.

3.1 Equations of Motion

The equations of motion of the new model are now derived by the Lagrangian mechanics. Let T, V and D denote the kinetic energy, the potential energy and the damping energy of the system, respectively. Then, these are

$$T = \frac{1}{2} m_s \dot{z}_s^2 + \frac{1}{2} m_u (\dot{y}_C^2 + \dot{z}_C^2) \tag{6a}$$

$$V = \frac{1}{2} k_s (\Delta l)^2 + \frac{1}{2} k_t (z_C - z_r)^2 \tag{6b}$$

$$D = \frac{1}{2} c_p (\dot{\Delta l})^2 \tag{6c}$$

Substituting the derivatives of (4e), (4f) and (5a,b,c) into (6a,b,c) yields

$$T = \frac{1}{2}(m_s + m_u)\dot{z}_s^2 + \frac{1}{2} m_u l_C^2 \dot{q}^2 + m_u l_C \cos q \dot{q}\, \dot{z}_s \tag{7a}$$

$$\begin{aligned} V = {} & \frac{1}{2} k_s [2a_l - b_l(\cos a' + \cos(a' - q)) - 2(a_l^2 - a_l b_l \\ & \cos a' + \cos(a' - q)) + b_l^2 \cos a' \cos(a' - q))^{1/2}] \\ & + \frac{1}{2} k_t [z_s + l_C(\sin(q - q_0) - \sin(-q_0) - z_r]^2 \end{aligned} \tag{7b}$$

$$D = \frac{c_p b_l^2 \sin^2(a' - q)\dot{q}}{8(a_l - b_l \cos(a' - q))} \tag{7c}$$

Finally, for the two generalized coordinates $q_1 = z_s$ and $q_2 = q$, the equations of motion are obtained as follows

$$\begin{aligned} & (m_s + m_u)\ddot{z}_s + m_u l_C \cos(q - q_0)\ddot{q} - m_u l_C \sin(q - q_0)\dot{q}^2 \\ & + k_t\left(z_s + l_C(\sin(q - q_0) - \sin(-q_0) - z_r\right) = -f_d \end{aligned} \tag{8}$$

$$\begin{aligned} & m_u l_C^2 \ddot{q} + m_u l_C \cos(q - q_0)\ddot{z}_s + \frac{c_p b_l^2 \sin(a' - q_0)\dot{q}}{4(a_l - b_l \cos(a' - q))} \\ & + k_t l_C \cos(q - q_0)(z_s + l_C(\sin(q - q_0) - \sin(-q_0)) - z_r) \\ & - \frac{1}{2} k_s \sin(a' - q)[b_l + \frac{d_l}{(c_l - d_l \cos(a' - q)^{1/2})}] = -l_B f_a \end{aligned} \tag{9}$$

where

$$c_l = a_l^2 - a_l b_l \cos(a + q_0) \text{ and } d_l = a_l b_l - b_l^2 \cos(a + q_0).$$

Now, introduce the state variables as $[x_1 \quad x_2 \quad x_3 \quad x_4]^T = [z_s \quad \dot{z}_s \quad q \quad \dot{q}]^T$. Then, (8)-(9) can be written in the state equation as follows.

$$\begin{aligned} \dot{x}_1 &= x_2 \\ \dot{x}_2 &= f_1(x_1, x_2, x_3, x_4, f_a, z_r, f_d) \\ x_3 &= x_4 \\ \dot{x}_4 &= f_2(x_1, x_2, x_3, x_4, f_a, z_r, f_d) \end{aligned} \tag{10}$$

where,

$$\begin{aligned} f_1 = \frac{1}{D_1}\{ & m_u l_C^2 \sin(x_3 - q_0) x_4^2 - \frac{1}{2} k_s \sin(a' - x_3)\cos(x_3 - q_0) g(x_3) \\ & + c_p h(x_3)\dot{q} - k_t l_C \sin^2(x_3 - q_0) z(\cdot) + l_B f_a \cos(x_3 - q_0) - l_C f_d \} \end{aligned}$$

$$\begin{aligned} f_2 = -\frac{1}{D_2}\{ & m_u^2 l_C^2 \sin(x_3 - q_0)\cos(x_3 - q_0) x_4^2 + (m_s + m_u) c_p h(x_3) x_4 \\ & - \frac{1}{2}(m_s + m_u) k_s \sin(a' - x_3) g(x_3) + m_s k_t l_C \cos(x_3 - q_0) z(\cdot) \\ & + (m_s + m_u) l_B f_a - m_u l_C \cos(x_3 - q_0) f_d \} \end{aligned}$$

and

$$D_1 = m_s l_C + m_u l_C \sin^2(x_3 - q_0)$$

$$D_2 = m_s m_u l_C^2 + m_u^2 l_C^2 \sin^2(x_3 - q_0)$$

$$g(x_3) = b_l + \frac{d_l}{(c_l - d_l \cos(a' - x_3))^{1/2}}$$

$$h(x_3) = \frac{b_l^2 \sin^2(a' - x_3)}{4(a_l - b_l \cos(a' - x_3))}$$

$$z(\cdot) = z(x_1, x_2, z_r) = x_1 + l_C(\sin(x_3 - q_0) - \sin(-q_0)) - z_r .$$

3.2 Linearization

In order to compare the characteristics of (10) with that of the conventional model, (10) is linearized at the equilibrium state where $x_e = (x_{1e}, x_{2e}, x_{3e}, x_{4e}) = (0,0,0,0)$. Then, the resulting linear equation is

$$\dot{x} = Ax(t) + B_1 f_a(t) + B_2 z_r(t) + B_3 f_d(t), \quad x(0) = x_0 \tag{11}$$

where

$$A = \begin{bmatrix} 0 & 1 & 0 & 0 \\ \frac{\partial f_1}{\partial x_1} & \frac{\partial f_1}{\partial x_2} & \frac{\partial f_1}{\partial x_3} & \frac{\partial f_1}{\partial x_4} \\ 0 & 0 & 0 & 1 \\ \frac{\partial f_2}{\partial x_1} & \frac{\partial f_2}{\partial x_2} & \frac{\partial f_2}{\partial x_3} & \frac{\partial f_2}{\partial x_4} \end{bmatrix}_{x_e} = \begin{bmatrix} 0 & 1 & 0 & 0 \\ a_{21} & 0 & a_{23} & a_{24} \\ 0 & 0 & 0 & 1 \\ a_{41} & 0 & a_{43} & a_{44} \end{bmatrix}$$

$$B_1 = \left[0 \quad \frac{\partial f_1}{\partial f_a} \quad 0 \quad \frac{\partial f_2}{\partial f_a} \right]^T_{f_a=0} = \begin{bmatrix} 0 \\ \dfrac{l_B \cos(-q_0)}{m_s l_C + m_u l_C \sin^2(-q_0)} \\ 0 \\ \dfrac{(m_s + m_u) l_B}{m_s m_u l_C^2 + m_u^2 l_C^2 \sin^2(-q_0)} \end{bmatrix}$$

$$B_2 = \left[0 \quad \frac{\partial f_1}{\partial z_r} \quad 0 \quad \frac{\partial f_2}{\partial z_r} \right]^T_{z_r=0} = \begin{bmatrix} 0 \\ \dfrac{k_t l_C \sin^2(-q_0)}{m_s l_C + m_u l_C \sin^2(-q_0)} \\ 0 \\ \dfrac{m_s k_t l_C \cos(-q_0)}{m_s m_u l_C^2 + m_u^2 l_C^2 \sin^2(-q_0)} \end{bmatrix}$$

$$B_3 = \left[0 \quad \frac{\partial f_1}{\partial f_d} \quad 0 \quad \frac{\partial f_2}{\partial f_d} \right]^T_{f_d=0} = \begin{bmatrix} 0 \\ \dfrac{l_C}{m_s l_C + m_u l_C \sin^2(-q_0)} \\ 0 \\ \dfrac{m_u l_C \cos(-q_0)}{m_s m_u l_C^2 + m_u^2 l_C^2 \sin^2(-q_0)} \end{bmatrix}$$

and

$$a_{21} = \frac{-k_t l_C \sin^2(-q_0)}{D_1}$$

$$\begin{aligned} a_{23} = \frac{1}{D_1^2}\{[\frac{1}{2}k_s(b_l + \frac{d_l}{(c_l - d_l\cos(a'))^{1/2}})(\cos(a'+q_0) \\ -\frac{1}{2}(k_s \sin a'\cos(-q_0)(\frac{d_l^2 \sin a'}{2(c_l - d_l \cos a')^{3/2}}) \\ -k_t l_C^2 \sin^2(-q_0)\cos(-q_0)]\cdot[m_s l_C + m_u l_C \sin^2(-q_0)] \\ + m_u k_s l_C \sin a' \sin(-q_0)\cos^2(-q_0)(b_l + \frac{d_l}{(c_l - d_l \cos a')^{1/2}})\} \end{aligned}$$

$$a_{24} = \frac{1}{D_1} \cdot \frac{c_p b_l^2 \sin^2 a'}{4(a_l - b_l \cos a')}$$

$$a_{41} = \frac{-m_s k_t l_C \cos(-q_0)}{D_2}$$

$$\begin{aligned} a_{43} = -\frac{1}{D_2^2}\{[\frac{1}{2}(m_s + m_u)k_s \cos a'(b_l + \frac{d_l}{(c_l - d_l\cos a')^{1/2}}) \\ -\frac{1}{2}(m_s + m_u)k_s \sin a'(\frac{d_l^2 \sin a'}{2(c_l - d_l \cos a')^{3/2}}) \\ + m_s k_t l_C^2 \cos(-q_0)]\cdot[m_s m_u l_C^2 + m_u^2 l_C^2 \sin^2(-q_0)] \\ + \frac{1}{2}(m_s + m_u)m_u^2 k_s l_C^2 \sin a' \sin(-q_0)(b_l + \frac{d_l}{(c_l - d_l \cos a')^{1/2}})\} \end{aligned}$$

$$a_{44} = -\frac{1}{D_2} \cdot \frac{(m_s + m_u) c_p b_l^2 \sin^2 a'}{4(a_l - b_l \cos a')}$$

Now, let the output variables be $y(t) = [\ddot{z}_s \quad q]^T$. Then the output equation is

$$y(t) = Cx(t) + D_1 f_a(t) + D_2 z_r(t) + D_3 f_d(t) \tag{12}$$

where,

$$C = \begin{bmatrix} a_{21} & 0 & a_{23} & a_{24} \\ 0 & 0 & 1 & 0 \end{bmatrix}, \quad D_1 = \begin{bmatrix} \dfrac{l_B \cos(-q_0)}{m_s l_C + m_u l_C \sin^2(-q_0)} \\ 0 \end{bmatrix},$$

$$D_2 = \begin{bmatrix} \dfrac{k_t l_C \sin^2(-q_0)}{m_s l_C + m_u l_C \sin^2(-q_0)} \\ 0 \end{bmatrix}, \quad D_3 = \begin{bmatrix} \dfrac{-l_C}{m_s l_C + m_u l_C \sin^2(-q_0)} \\ 0 \end{bmatrix}.$$

4. Comparison of Two Models

In the conventional model, where the road input is $\dot{z}_r$, the output variables were assumed to be the accelerations of the sprung mass $\ddot{z}_s$ and the unsprung mass $\ddot{z}_u$. In (12), however, while the road input is the displacement z_r, the outputs are the acceleration of the sprung mass $\ddot{z}_s$ and the angular displacement of the control arm q. Thus, the output variable that can be compared between the two models is the acceleration of the sprung mass $\ddot{z}_s$. To be able to compare the two models, the road input in the new model is modified to the velocity $\dot{z}_r$.

First, it is shown that the conventional model and the new model coincide if the lower support point of the shock absorber in the new model is located at the mass center of the unsprung mass. Let $l_B = l_C$, $l_B = l_A \cos a$ and $q_0 = 0^\circ$. Then, equation (11) has the form

$$\dot{x} = Ax(t) + B_1 f_a(t) + B_2 z_r(t) + B_3 f_d(t), \quad x(0) = x_0 \tag{11}'$$

where,

$$A = \begin{bmatrix} 0 & 1 & 0 & 0 \\ 0 & 0 & \dfrac{k_s l_C}{m_s} & \dfrac{c_p l_C}{m_s} \\ 0 & 0 & 0 & 1 \\ -\dfrac{k_t}{m_u l_C} & 0 & -\dfrac{(m_s + m_u) k_s}{m_u m_s} - \dfrac{k_t}{m_u} & -\dfrac{(m_s + m_u) c_p}{m_s m_u} \end{bmatrix},$$

$$B_1 = \begin{bmatrix} 0 & \dfrac{1}{m_s} & 0 & -\dfrac{m_s + m_u}{m_s m_u l_C} \end{bmatrix}^T, \quad B_2 = \begin{bmatrix} 0 & 0 & 0 & \dfrac{k_t}{m_u l_C} \end{bmatrix}^T, \quad B_3 = \begin{bmatrix} 0 & -\dfrac{1}{m_s} & 0 & \dfrac{1}{m_s l_C} \end{bmatrix}^T.$$

The output equation of (12) becomes

$$y(t) = Cx(t) + D_1 f_a(t) + D_3 f_d(t) \tag{12}'$$

where,

$$C = \begin{bmatrix} 0 & 0 & \dfrac{k_s l_C}{m_s} & \dfrac{c_p l_C}{m_s} \\ 0 & 0 & 1 & 0 \end{bmatrix}, \quad D_1 = \begin{bmatrix} \dfrac{1}{m_s} \\ 0 \end{bmatrix}, \quad D_3 = \begin{bmatrix} -\dfrac{1}{m_s} \\ 0 \end{bmatrix}.$$

For the above equations (11)′ and (12)′, the transfer function from a road velocity input sz_r to the acceleration of the sprung mass is exactly the same as (3). That is, the conventional model, as such, is a special case of the new model where $l_B = l_C$ and $q_0 = 0$. Thus, the new model is more general, from the point of view that it has an extra degree of freedom in validating the real plant with experimental data.

For comparing the two models, the following parameter values of a typical Macpherson type suspension system are used:

$$m_s = 453Kg, \quad m_u = 71Kg, \quad c_p = 1950N \cdot \sec/m,$$

$$k_s = 17{,}658N/m, k_t = 183{,}887N/m, \quad f_d = 0N,$$
$$l_A = 0.66m, \quad l_B = 0.34m, \text{ and } \quad l_C = 0.37m.$$

As compared in Table 1, the first frequency of the conventional model is located below 1 Hz, whereas the that of the new model is located at 1.25 Hz. Since the real plant has its first resonance frequency at 1.2 Hz, the results of the new model better agree with the experimental results. As it is important to decrease the resonance peak near 1 Hz to improve the ride quality, it is claimed that the new model, which reveals the exact locations of resonance frequencies, is a better model.

Table 1. Comparison of the two models for a typical suspension system

	Conventional model	New model	
		$l_B = l_C$	$l_B = 0.34m$ $l_C = 0.37m$
Poles	-1.85±5.79I -14.04±50.40i	-1.85±5.79i -14.04±50.40i	-1.50±7.70i -10.92±48.30i
Resonances (Damping ratio)	0.97 Hz (0.30) 8.33 Hz (0.27)	0.97 Hz (0.30) 8.33 Hz (0.27)	1.25 Hz (0.20) 7.88 Hz (0.23)

The frequency responses of the two models, with the same road input, are compared in Fig. 5. There are substantial differences in the resonance frequencies and peaks between the two models. A tendency of the new model is that the smaller the l_C / l_B is, the lower the resonance frequency is. All the above observations are summarized as follows:

(1) The conventional model is considered as a special case of the new model where $l_B = l_C$.

(2) The location of the first resonance frequency is higher in the new model than it is in the conventional one. This better agrees with the experimental results. The damping ratio, however, is lower in the new model.

(3) For the second resonance frequency, both the location and the damping ratio are lower in the new model.

5. Optimal Pole-Placement Control: Active Case

In this section, an optimal pole-placement control which combines the LQ control and the pole-placement technique for the new model is presented. The closed loop system is designed to have desired characteristics by means of the pole-placement technique, while minimizing the cost function, as defined by the weightings of the input, state and output of the system, as follows.

The considered linear time-invariant system and the performance index are

$$\dot{x} = Ax + B_1 u + B_2 z_r, \qquad x \in R^n, \qquad u \in R^m \tag{13}$$

$$J = \frac{1}{2}\int_0^\infty \{x^T Q x + u^T R u\} dt, \qquad Q \geq 0, \qquad R > 0 \tag{14}$$

where A, B_1 and B_2 are defined in (11). For given Q and R, the optimal control law and the optimal closed loop system are

$$u = -R^{-1} B_1{}^T M_s x \stackrel{\Delta}{=} -Kx \tag{15}$$

$$\dot{x} = (A - B_1 R^{-1} B_1{}^T M_s) x \stackrel{\Delta}{=} Fx \tag{16}$$

where $M_s \geq 0$ is the solution of the Riccati equation below.

$$A^T M_s + M_s A - M_s B_1 R^{-1} B_1^T M_s + Q = 0 \tag{17}$$

The solution of the Riccati equation, M_s, can be obtained in another approach as follows. Let $S = B_1 R^{-1} B_1{}^T$. Introduce a Hamiltonian matrix H as

$$H = \begin{bmatrix} A & -S \\ -Q & -A^T \end{bmatrix} \tag{18}$$

The Jordan decomposition of H is of the form

$$HX = X\Lambda$$

where X and Λ contain the eigenvectors and the eigenvalues of H, respectively. Then, the following relationship is known [9].

$$H \begin{bmatrix} X_s & X_u \\ Y_s & Y_u \end{bmatrix} = \begin{bmatrix} X_s & X_u \\ Y_s & Y_u \end{bmatrix} \begin{bmatrix} \Lambda(F) & 0 \\ 0 & \Lambda_u \end{bmatrix} \tag{19}$$

where F is the closed loop system matrix defined in (16), $\Lambda(F)$ denotes an eigen matrix in which the eigenvalues of F appear in diagonal terms, $\Lambda_u = -\Lambda(F)$, $\begin{bmatrix} X_s^T & Y_s^T \end{bmatrix}^T$ consists of the eigenvectors of H corresponding to the eigenvalues of F, and $\begin{bmatrix} X_u^T & Y_u^T \end{bmatrix}^T = -\begin{bmatrix} X_s^T & Y_s^T \end{bmatrix}^T$. Furthermore, M_s and M_u are determined as follows.

$$M_s = Y_s X_s^{-1} \tag{20}$$

$$M_u = Y_u X_u^{-1} \tag{21}$$

where $M_u = -M_s$.

In the problem of shifting the eigenvalues of the closed loop system by $-2a$ further to the left, where the a is said to be the degree of relative stability of the optimal pole-placement problem, the following theorem holds.

Theorem[9]: For given Q and R let Λ_s be the spectrum of optimal system (16). Let the degree of relative stability be $a = p$. Let Q be perturbed by

$$\Delta Q = -2pM_u \tag{22}$$

where M_u is the negative (semi) definite solution given by (21). Then, $\Lambda(F_p)$, the spectrum of the optimal closed system obtained with the modified weighting matrix, $Q_p = Q + \Delta Q$, is

$$\Lambda(F_s) = \Lambda_s - 2pI \tag{23}$$

where F_p denotes the closed loop system matrix resulted from Q_p. ¡ à

Design Procedure

1) Select Q and R, and design a LQR controller.

2) Evaluate the performance of the LQR controller, and determine the eigenvalues that need to be shifted.

3) Construct the Hamiltonian matrix H, and find the eigenvectors of H corresponding to the eigenvalues that need to be shifted.

4) Obtain

$$M_i = Y_i X_i^{-1} \tag{24}$$

where $\begin{bmatrix} X_i & Y_i \end{bmatrix}^T$ is the matrix that is composed of the unstable eigenvectors corresponding to the eigenvalues that need to be shifted, and the stable eigenvectors corresponding to the eigenvalues that stay in their original locations.

5) Let p_i be the degree of relative stability of the eigenvalues that are to be shifted. Calculate

$$A_i = A_{i-1} + p_i I, \quad \text{where } A_0 = A \tag{25}$$

$$Q_i = Q_{i-1} - 2p_i M_i, \text{ where } Q_0 = Q \tag{26}$$

6) Solve the Riccati equation with the modified matrices, or try the second method (20),

to obtain the desired closed loop pole locations.

5.1 LQR

In this paper, it is assumed that the main purpose of the control system design is to improve the ride quality. Thus, to reduce the vertical acceleration of the sprung mass at the resonance frequency near 1 Hz, more weights are put on the state variables x_1 and x_2 that correspond to the displacement and velocity of the sprung mass. The weighting matrices initially selected are

$$Q = diag(10^5 \quad 10^5 \quad 10^{-1} \quad 10^{-1}) \qquad R = 10^{-2} \tag{27}$$

The closed loop eigenvalues with (27) are

$$l_C = \{-3.2042 \pm 7.1971i, \quad -10.8560 \pm 48.2377i\}.$$

Compared to the open loop system, the resonance peak near 1 Hz of the controlled system is lower. Due to length considerations, simulation results for (27) are omitted.

5.2 Optimal Pole-placement

In this section, the damping ratios of the two dominant poles are raised for the purpose of increasing the rise time. The damping ratio of the first resonance frequency is increased from 0.407 to 0.841 by shifting the dominant pole, by –8, to the left. Therefore, the eigenvalues of the closed loop system are

$$l_{opt} = \{-11.2042 \pm 7.1971i, \quad -10.8560 \pm 48.2377i\}.$$

Fig. 6 compares the frequency responses of the open loop system and the optimal pole-placement controller. It is shown that the performance in the low frequency range, including 1 Hz, has been significantly improved with the optimal pole-placement controller. Fig. 7 shows the time domain responses when passing over a speed bump which is $10cm$ in height and $0.\ m$ in length. Also, note the great improvement in the settling time.

6. Application to a Semi-Active Damper

In this section, the optimal pole-placement technique, discussed in Section 5, is applied to a semi-active damper. The purpose of this section is to figure out how much the control performance of the active control is degraded when the control law, derived for an active actuator, is applied to a plant with a semi-active actuator.

If the actuator in Fig. 4 is a semi-active type, the passive damper and the actuation part involving the arrow sign need to be combined as one variable damper. In deriving the equations of motion for a semi-active damper, the equation of motion for the coordinate z_r is the same as equation (8). However, the equation of motion for q needs to be modified as follows.

$$\begin{aligned} & m_u l_C^2 \ddot{q} + m_u l_C \cos(q - q_0)\ddot{z}_s + \frac{c_s b_l^2 \sin(a' - q_0)\dot{q}}{4(a_l - b_l \cos(a' - q))} \\ & + k_t l_C \cos(q - q_0)(z_s + l_C(\sin(q - q_0) - \sin(-q_0)) - z_r) \\ & - \frac{1}{2} k_s \sin(a' - q)[b_l + \frac{d_l}{(c_l - d_l \cos(a' - q)^{1/2})}] = -l_B f_{sa} \end{aligned} \tag{28}$$

where f_{sa} stands for a semi-active control force. The system matrix A of (11) needs to be modified as follows.

$$A = \begin{bmatrix} 0 & 1 & 0 & 0 \\ a_{21} & 0 & a_{23} & 0 \\ 0 & 0 & 0 & 1 \\ a_{41} & 0 & a_{43} & 0 \end{bmatrix} \tag{29}$$

where a_{21}, a_{23}, a_{41} and a_{43} are the same as in Section 3.2.

6.1 Continuously Variable Damper

Fig. 8 shows the damping force characteristics of a typical continuously variable damper used for the simulations in this paper. Detailed descriptions for the variable damper are omitted. In general, the damping force of a semi-active damper is adjusted by changing the size of an orifice. In Fig. 8, the x-axis represents the relative velocity of the rattle space, and the y-axis denotes the generated damping force. The three curves represents three different damping force characteristics corresponding to the three current inputs of 0 ampere, 0.8 ampere, and 1.6 ampere. The curve with the highest slope denotes the characteristics of 0 ampere control input, which denotes the most hard damping effect.

6.2 Limited Control Action

Control law (15) assumes that there are no limits, in terms of the magnitude and the direction, to the control input. However, if a semi-active type actuator of Section 6.1 is used, the actuating force is limited as follows

$$f_{actual} = \begin{cases} \overline{f}_{sa} & if \quad u \geq \overline{f}_{sa} \\ u & if \quad \underline{f}_{sa} < u < \overline{f}_{sa} \\ \underline{f}_{sa} & if \quad u \leq \underline{f}_{sa} \end{cases} \tag{30}$$

where $\overline{f}_{sa}$ and $\underline{f}_{sa}$ denote the maximum and the minimum damping forces at a given relative velocity. As, for example, in Fig. 8 when the rattle space is extended at a relative velocity $1\,m/\sec$, the maximum damping force is about 2700 N. This corresponds to 0A. At the same time the minimum damping force is about 1400 N, which corresponds to 1.6A.

Fig. 9 compares the accelerations of the sprung mass of passive, semi-active and active suspension systems, when the magnitude and the frequency of the road input are $0.01\,m$ and 1 Hz. Compared to the passive system, both the semi-active and the active systems show a reduction in the magnitude of the vertical acceleration. Therefore, it is concluded that the control law, derived for an active suspension system, may be applicable to a semi-active suspension system without resulting in much degradation of control performance. Fig. 10 compares the control forces applied to the plant by the active and semi-active dampers together with the relative velocity of the damper. In the case of the semi-active damper, the occurrence of the phase lag is due to the actuation limitation. This also causes the phase difference in the response of the sprung mass acceleration in Fig. 9. Fig. 11 shows the current input applied to the continuously variable semi-active damper of Fig. 8.

7. Conclusions

In this paper a new control-oriented model, for the Macpherson type suspension system, that incorporates the rotational motion of the control arm was investigated for the first time. The nonlinear equations of motion have been linearized at an equilibrium point. It was shown that the conventional model is a special case of the new model, i.e., if $l_B = l_C$ and $q_0 = 0$, then the transfer function of the new model coincides exactly with that of the conventional model. By changing the length of the control arm, it is possible to design a wide range of plant models. An optimal pole-placement controller, which combines the LQ control and the pole-placement method, was investigated. The control law was further applied to a semi-active suspension equipped with a continuously variable damper. When the active control law was applied to the semi-active damper, a small degradation in the vertical acceleration of the sprung mass was noticed. However, the overall performance was acceptable. The new model proposed in this paper has applications in the areas of dynamics analysis and control system design.

References

K. S. Lee, M. W. Suh, and T. I. Oh (1994). "A Robust Semi-active Suspension Control Law (with English abstract)," *Korea Society of Automotive Engineers*, Vol. 2, No. 6, pp.117-126.

S. J. Huh (1996). "Active Chassis Systems for Automotives (with English abstract)," *Journal of Control, Automation and Systems Engineering*, Vol. 2, No. 2, pp. 57-65.

A. Alleyne and J. K. Hedrick (1995). "Nonlinear Adaptive Control of Active Suspensions," *IEEE Transaction on Control Systems Technology*, Vol. 3, No. 1, pp. 94-101.

H. Kim and Y. S. Yoon (1995). "Semi-Active Suspension with Preview Using a Frequency-Shaped Performance Index," *Vehicle System Dynamics*, 24, pp. 759-780.

A. J. Truscott and P. E. Wellstead (1995). "Adaptive Ride Control in Active Suspension Systems," *Vehicle System Dynamics*, 24, pp. 197-230.

S. R. Teja and Y. G. Srinivasa (1996). "Investigation on the Stochastically Optimized PID Controller for a Linear Quarter-Car Road Vehicle Model," *Vehicle System Dynamics*, 26, pp. 103-116.

M. Jonsson (1991). "Simulation of Dynamical Behaviour of a Front Wheel Suspension," *Vehicle System Dynamics*, 20, pp. 269-281.

A. Stensson, C. Asplund and L. Karlsson (1994). "The Nonlinear Behaviour of a MacPerson Strut Wheel Suspension," *Vehicle System Dynamics*, 23, pp. 85-106.

J. Medanic, H. S. Tharp and W. R. Perkins (1988). "Pole Placement by Performance Criterion Modification," *IEEE Transactions on Automatic Control*, Vol. 33, No. 5, pp. 469-472.

C. Yue, T. Butsuen and J. K. Hedrick (1989). "Alternative Control Laws for Automotive Active Suspension," *Transactions of the ASME, Journal of Dynamics System, Measurement, and Control*, Vol. 111, pp. 286-291.

J. S. Lin and I. Kanellakopoulos (1997). "Nonlinear Design of Active Suspensions," *IEEE Control System Magazine*, Vol. 17, No. 3, pp 45-59.

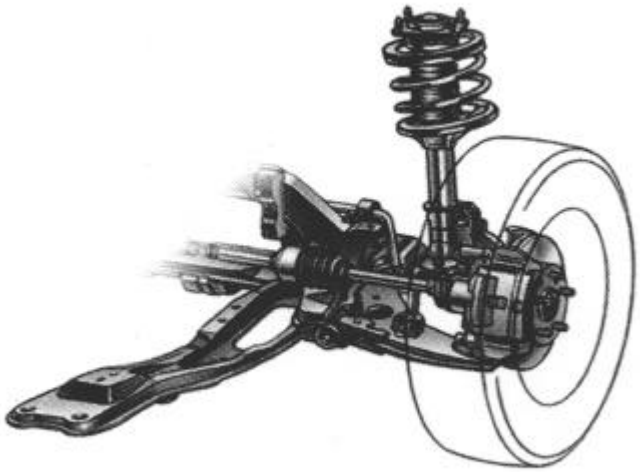

Fig. 1 A sketch of the Macpherson strut wheel suspension

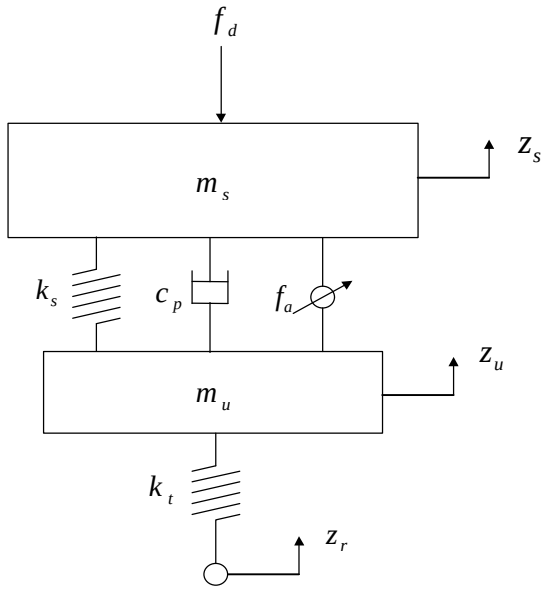

Fig. 2 Conventional quarter car model.

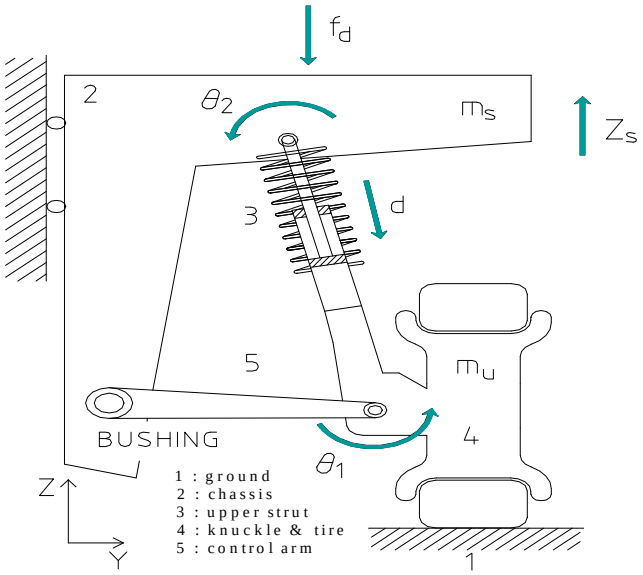

Fig. 3 A schematic diagram of the Macpherson type suspension system.

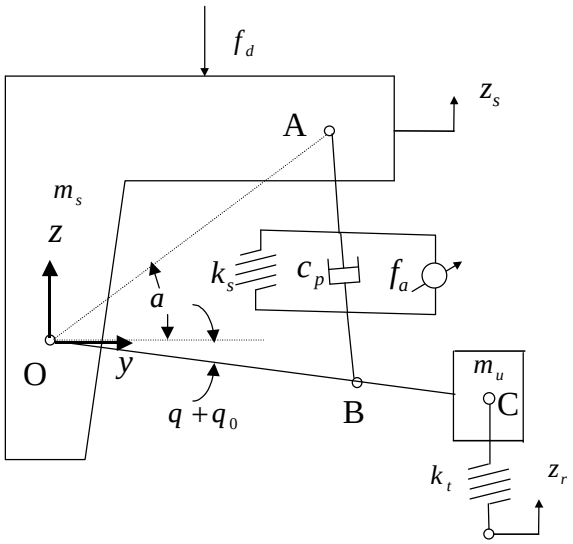

Fig. 4 A new quarter car model.

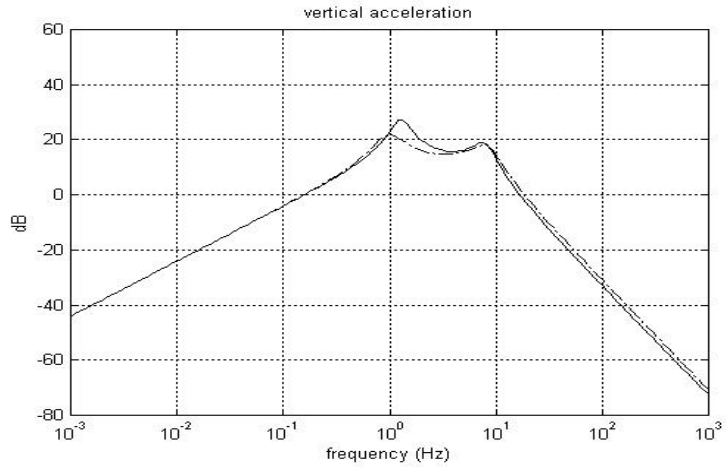

(··· conventional model, — new model)

Fig. 5 Frequency responses of the conventional and new models.

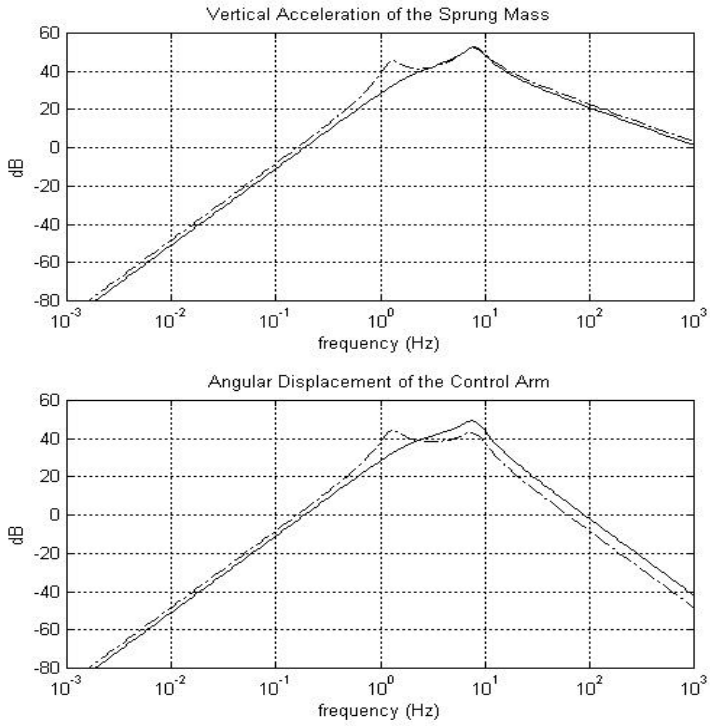

(··· open loop system, — optimal pole-placement)

Fig. 6 Comparison of the frequency responses.

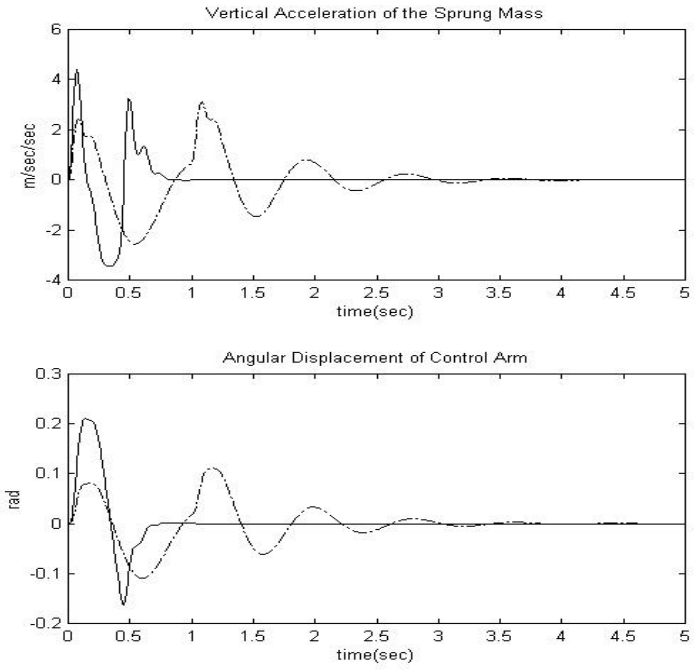

(··· open loop system, — optimal pole-placement)

Fig. 7 Comparison of the time domain responses.

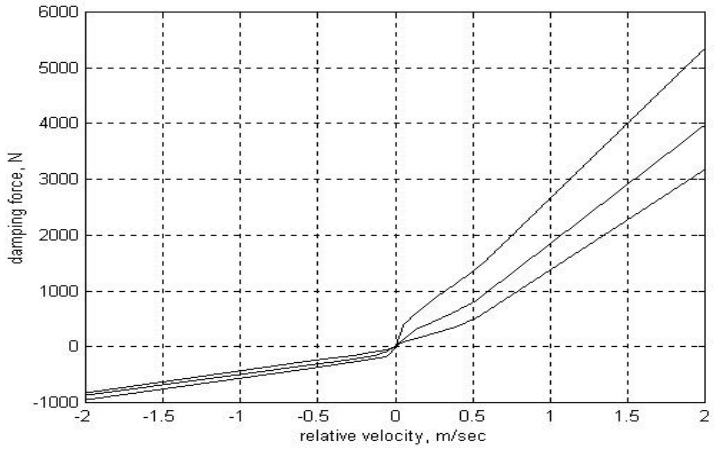

Fig. 8 Damping force characteristics of a typical continuously variable damper.

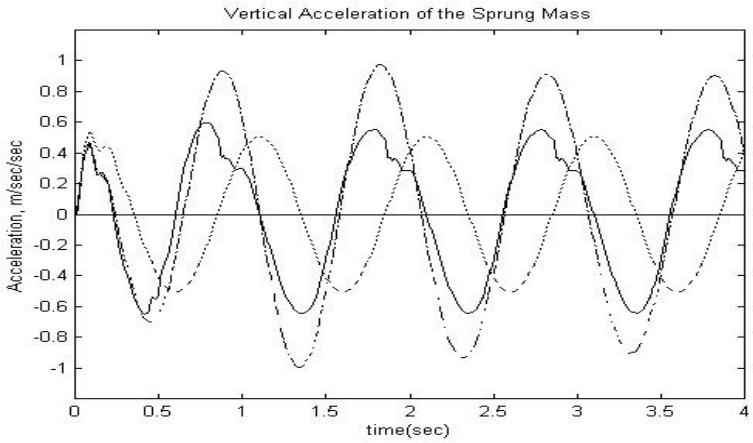

(-·- passive, — semi-active, ··· active)

Fig. 9 Comparison of passive, semi-active, and active suspension systems.

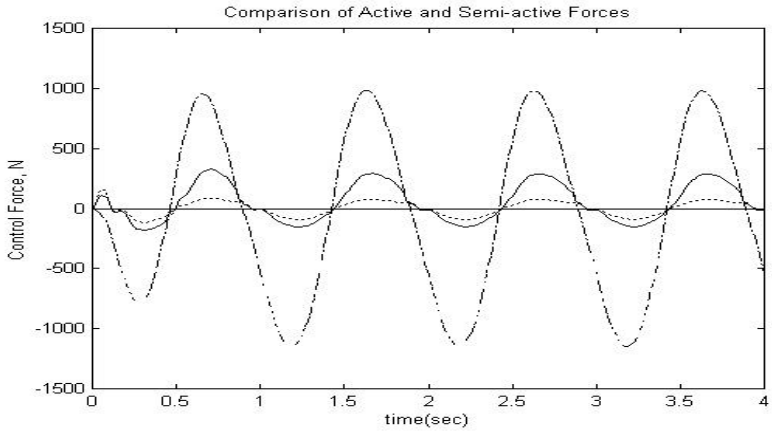

(-·- active control force(desired), — semi-active damping force(generated), ··· relative velocity of the damper)

Fig. 10 Control forces.

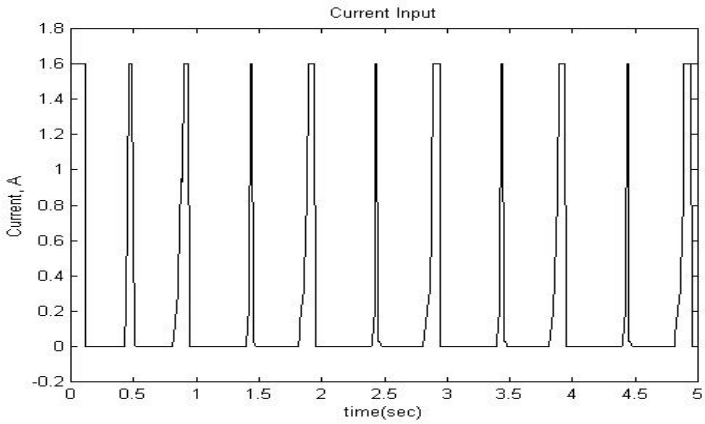

Fig. 11 Current input applied to the continuously-variable damper in Fig. 8.